

described for $\{\eta^3\text{-HB(3-Bu}^i\text{pz)}_3\}_3\text{FeCl}$. The intensity of 3451 unique reflections in the range $3 \leq 2\theta \leq 58^\circ$ (h, k, l) were measured, of which 1249 with $F > 6\sigma(F)$ were used in the structure determination. Systematic absences were consistent with either $Pnma$ or $Pna2_1$ space groups, but E -value statistics strongly favored the centrosymmetric alternative, $Pnma$. Most of the hydrogen atoms were located in the difference map after all the non-hydrogen atoms were located and refined anisotropically, but hydrogens on carbon were allowed to refine in calculated positions ($d_{\text{C-H}} = 0.96 \text{ \AA}$; $U_{\text{iso}}(\text{H}) = 1.2U_{\text{iso}}(\text{C})$). Block-diagonal least-squares refinement converged to $R = 4.54$ ($R_w = 4.85$) with a goodness-of-fit = 1.21 for 155 parameters. The final difference map showed no significant features, with the highest final peak 0.37 e \AA^{-3} . Atomic coordinates and thermal parameters for non-hydrogen atoms are listed in Table IV, and selected bond distances and angles are listed in Tables V and VI.

X-ray Structure Determinations of $\{\eta^3\text{-HB(3-Bu}^i\text{pz)}_3\}_3\text{CoF}$. Crystal data, data collection, and refinement parameters are summarized in Table X. Intensity data collection and processing procedures are as described for $\{\eta^3\text{-HB(3-Bu}^i\text{pz)}_3\}_3\text{FeCl}$, with the exception that an absorption correction was not applied. The intensity of 3833 unique reflections in the range $3 \leq 2\theta \leq 60^\circ$ ($h, k, \pm l$) were measured, of which

2319 with $F > 6\sigma(F)$ were used in the structure determination. Systematic absences were consistent with either the $P1n1$ or $P12/n1$ space group, but E -value statistics strongly favored the noncentrosymmetric alternative, $P1n1$. Most of the hydrogen atoms were located in the difference map after all the non-hydrogen atoms were located and refined anisotropically, but hydrogens on carbon were allowed to refine in calculated positions ($d_{\text{C-H}} = 0.96 \text{ \AA}$; $U_{\text{iso}}(\text{H}) = 1.2U_{\text{iso}}(\text{C})$). Block-diagonal least-squares refinement converged to $R = 4.79$ ($R_w = 5.74$) with a goodness-of-fit = 1.29 for 273 parameters. The final difference map showed no significant features, with the highest final peak 0.62 e \AA^{-3} . Atomic coordinates and thermal parameters for non-hydrogen atoms are listed in Table VII, and selected bond distances and angles are listed in Tables VIII and IX.

Supplementary Material Available: Tables SI–SIX, listing crystal and intensity collection data, hydrogen atomic coordinates, and anisotropic displacement parameters for $\{\eta^3\text{-HB(3-Bu}^i\text{pz)}_3\}_3\text{FeCl}$, $\{\eta^3\text{-HB(3-Bu}^i\text{pz)}_3\}_3\text{CoCl}$, and $\{\eta^3\text{-HB(3-Bu}^i\text{pz)}_3\}_3\text{CoF}$ (9 pages); tables of calculated and observed structure factors (28 pages). Ordering information is given on any current masthead page.

Contribution from the Department of Chemistry,
Frick Laboratory, Princeton University, Princeton, New Jersey 08544-1009

Multielectron Transfer and Single-Crystal X-ray Structure of a Trinuclear Cyanide-Bridged Platinum–Iron Species

Meisheng Zhou, Brian W. Pfennig, Jana Steiger, Donna Van Engen, and Andrew B. Bocarsly*

Received October 19, 1989

$[\text{Pt}(\text{NH}_3)_4]_2[(\text{NC})_5\text{Fe}^{\text{II}}\text{-CN-Pt}^{\text{IV}}(\text{NH}_3)_4\text{-NC-Fe}^{\text{II}}(\text{CN})_5] \cdot 9\text{H}_2\text{O}$ was synthesized by the redox reaction of $\text{Pt}(\text{NH}_3)_4(\text{NO}_3)_2$ and $\text{K}_3\text{Fe}(\text{CN})_6$ in aqueous solution. The red complex crystallized in space group $P2_1/c$ (No. 14) and was analyzed by X-ray diffractometry. The monoclinic crystal consists of a trinuclear, cyanide-bridged Fe–Pt–Fe anion hydrogen-bonded via a terminal cyanide group on each iron atom to two separate tetraammineplatinum(II) counterions. Unit cell dimensions are $a = 15.313$ (2) \AA , $b = 8.5353$ (14) \AA , $c = 16.206$ (5) \AA , $\beta = 100.52$ (2)°, and $Z = 2$; a center of inversion exists at the central Pt atom of the trinuclear anion. The R factors for this structure are $R = 5.0\%$ and $R_w = 5.3\%$. On the basis of infrared spectroscopy, magnetic measurements, ESR spectroscopy, and the electrochemistry of the compound, localized oxidation states of $\text{Fe}^{\text{II}}\text{-Pt}^{\text{IV}}\text{-Fe}^{\text{II}}$ are assigned to the complex. The electronic spectrum reveals an intervalent (IT) charge-transfer absorption at approximately 470 nm. Excitation into this band effects an electron transfer between the Fe^{II} and Pt^{IV} atoms and results in the formation of $\text{Pt}(\text{NH}_3)_4^{2+}$ and ferricyanide in a 1 to 2 ratio. The initial quantum yield for the formation of ferricyanide at 488-nm irradiation is 0.02.

Introduction

Inorganic donor/acceptor complexes containing intervalent (IT) or metal to metal charge-transfer (MMCT) bands have received significant attention in the last decade due to their potential applications to solar energy conversion and/or photocatalysis. Homobinuclear mixed-valent transition-metal complexes, particularly those of ruthenium, have been extensively investigated.¹ These compounds exhibit IT absorptions at low energies, whereas these transitions often occur in the visible region of the spectrum in the heterobinuclear complexes due to the redox asymmetry of the metal centers.² Inorganic donor/acceptor complexes can be classified into two general types: contact ion pairs and linkage isomers. Binuclear examples of both types have been well characterized. Cyanide is often employed as a bridging ligand since MLCT bands with this ligand occur at high energies and do not obscure the observation of IT transitions in the visible electronic spectrum.³ Many of the cyanide-bridged species have been demonstrated to undergo inner sphere electron transfer upon irradiation into their respective IT absorption bands.⁴ However, only a handful of intervalent transition-metal complexes containing three (or more) metal centers have been characterized,^{5,6} and none of these, to the best of our knowledge, demonstrate photochemistry involving all three metals. Furthermore, the detailed structures of these multinuclear species have never been determined. We herein report the synthesis, characterization, chemistry, and crystal structure of the trinuclear, cyanide-bridged complex $\{[\text{Pt}$

$(\text{NH}_3)_4]_2^{4+}\}[(\text{NC})_5\text{Fe}^{\text{II}}\text{-CN-Pt}^{\text{IV}}(\text{NH}_3)_4\text{-NC-Fe}^{\text{II}}(\text{CN})_5]^{4-}\} \cdot 9\text{H}_2\text{O}$. Not only does this complex exhibit an IT absorption in the visible region of the optical spectrum, but we find that irradiation into this absorption leads to a two-electron charge transfer involving all three metal centers.

Vogler et al. have recently reported the synthesis of the trinuclear compound $[(\text{bpy})(\text{H}_2\text{O})\text{Pt}^{\text{II}}\text{-NC-M}^{\text{II}}(\text{CN})_4\text{-CN-Pt}^{\text{II}}(\text{bpy})(\text{H}_2\text{O})]$ (where $\text{M} = \text{Fe, Ru, or Os}$ and $\text{bpy} = 2,2'$ -bipyridine),⁵ which holds a superficial similarity to the complex reported. Unlike the complex under consideration, this compound contains all three metals in their lowest formal oxidation states and was characterized solely by MLCT ($\text{M}^{\text{II}} \rightarrow \pi^*\text{-bpy}$) absorptions. Consistent with this spectral assignment, the complex

- (1) (a) Taube, H. *Ann. N.Y. Acad. Sci.* **1978**, *313*, 483. (b) Meyer, T. J. *Ann. N.Y. Acad. Sci.* **1978**, *313*, 496. (c) Meyer, T. J. *Acc. Chem. Res.* **1978**, *11*, 94. (d) Meyer, T. J. In *Mixed-Valence Compounds*; Brown, D. B., Ed.; NATO Advanced Study Institute Series, No. 58; Reidel: Dordrecht, The Netherlands, 1980. (e) Creutz, C. *Prog. Inorg. Chem.* **1983**, *30*, 1.
- (2) Vogler, A.; Osman, A. H.; Kunkely, H. *Coord. Chem. Rev.* **1985**, *64*, 159.
- (3) Lever, A. B. P. *Inorganic Electronic Spectroscopy*; Elsevier: Amsterdam, 1985.
- (4) (a) Vogler, A.; Kunkely, H. *Ber. Bunsen-Ges. Phys. Chem.* **1975**, *79*, 83. (b) Vogler, A.; Kunkely, H. *Ber. Bunsen-Ges. Phys. Chem.* **1975**, *79*, 301. (c) Vogler, A.; Osman, A. H.; Kunkely, H. *Inorg. Chem.* **1987**, *26*, 2337. (d) Vogler, A.; Kisslinger, J. *J. Am. Chem. Soc.* **1982**, *104*, 2311.
- (5) Vogler, A.; Kunkely, H. *Inorg. Chim. Acta* **1988**, *150*, 1.
- (6) Bigozzi, C. A.; Roffia, S.; Scandola, F. *J. Am. Chem. Soc.* **1985**, *107*, 1644.

* To whom correspondence should be addressed.

is reported to undergo photoinduced charge transfer. However, this reaction is one electron in nature and only occurs at localized metal centers.

Experimental Section

Preparation of $C_{12}H_{12}Fe_2N_{16}Pt(N_4H_{12}Pt)_2 \cdot 9H_2O$. Tetraammineplatinum(II) nitrate and potassium ferricyanide were obtained from Aldrich and used without further purification. These were dissolved in distilled water, combined in a 3:2 molar ratio, respectively (approximately 0.08 M total concentration), and stored in the dark. Within minutes, the solution turned a deep red color and a new band appeared in the electronic absorption spectrum. A red-orange precipitate formed after several hours and was filtered out by vacuum, washed with distilled water, and dried on a watch glass at room temperature.

Apparatus. UV-vis spectroscopy was performed by using an HP 8450A diode-array spectrophotometer, and infrared spectra were recorded from KBr pellets in the 4000–400- cm^{-1} range on a Perkin-Elmer 1710 FTIR instrument equipped with a Series 3600 data station. A Princeton Applied Research (PAR) Model 173 potentiostat with a PAR 175 universal programmer and an XY recorder was employed for the electrochemical studies; a Coherent Innova 70 Ar ion laser operating at 488 nm was used for the photochemical experiments. ESR spectroscopy was performed on an ER200D X-band EPR spectrometer at 9.37 GHz microwave frequency (298 K), scanning the range 0–5000 G and using potassium ferricyanide as a test standard. Magnetic susceptibility measurements were made with a Johnson Matthey balance; Mohr's salt was used as the standard.

Crystal Structure Determination. Single-crystal X-ray diffraction data were obtained with a Nicolet R3m diffractometer equipped with a graphite crystal monochromator. Initial attempts to collect data at low temperature (230 K) resulted in decomposition of the crystal. It was noted that the crystals maintained at room temperature were stable, and therefore, further manipulations were carried out at room temperature. Unit cell constants were determined by a least-squares fit of the 2θ values of 18 reflections having $25^\circ \leq 2\theta \leq 30^\circ$. The standard reflections used to monitor data collection showed no decline in intensity over the period of accumulation. Raw intensities were reduced to structure factor amplitudes by correction for scan speed, background, Lorentz, and polarization effects. Azimuthal data were collected for 11 reflections representing the range of 2θ values, the principal crystal face was indexed (100), and a lamina empirical absorption correction was applied to the data set. The structure was solved by using standard heavy-atom techniques in the SHELXTL package of programs.⁷ The 4- anion is centered at an inversion site with one $Pt(NH_3)_4^{2+}$ counterion per asymmetric unit. Following refinement with isotropic temperature factors, several large peaks were observed in a difference Fourier map. They were assigned as water solvent molecules. A total of five positions were located for water per asymmetric unit, four of which were refined at full occupancy and the other [O(5)] at half-occupancy. Hydrogen atoms were not included. In the final stages of refinement, all non-hydrogen atoms were refined with anisotropic temperature factors. The largest residual electron density peaks were in the vicinity of the Pt atoms or the solvent molecules. The analytical scattering factors for the neutral atoms were used, and all non-hydrogen scattering factors were corrected for both the real and imaginary components of anomalous dispersion.⁸

Results and Discussion

Synthesis and Characterization. When tetraammineplatinum(II) nitrate and potassium ferricyanide were combined in aqueous solution, the initially yellow solution slowly turned a deep red color over several minutes. After several hours, a red-orange precipitate was formed, which could be filtered out by vacuum in cases where a 3:2 molar ratio of the above reagents was employed. This dissolved appreciably in distilled water only if ground by a mortar and pestle. Diffraction-quality single crystals were found to grow in a diluted solution of the reactants.

The infrared spectrum of the solid in the cyanide stretching frequency region contains two groups of absorptions—the first, centered at 2055 cm^{-1} , is assigned to terminal cyanide stretches in the Fe^{II} oxidation state, while those centered at 2125 cm^{-1} are associated with bridging cyanide groups, by analogy with the assignments of other cyanide-bridged species.⁹ Upon complex

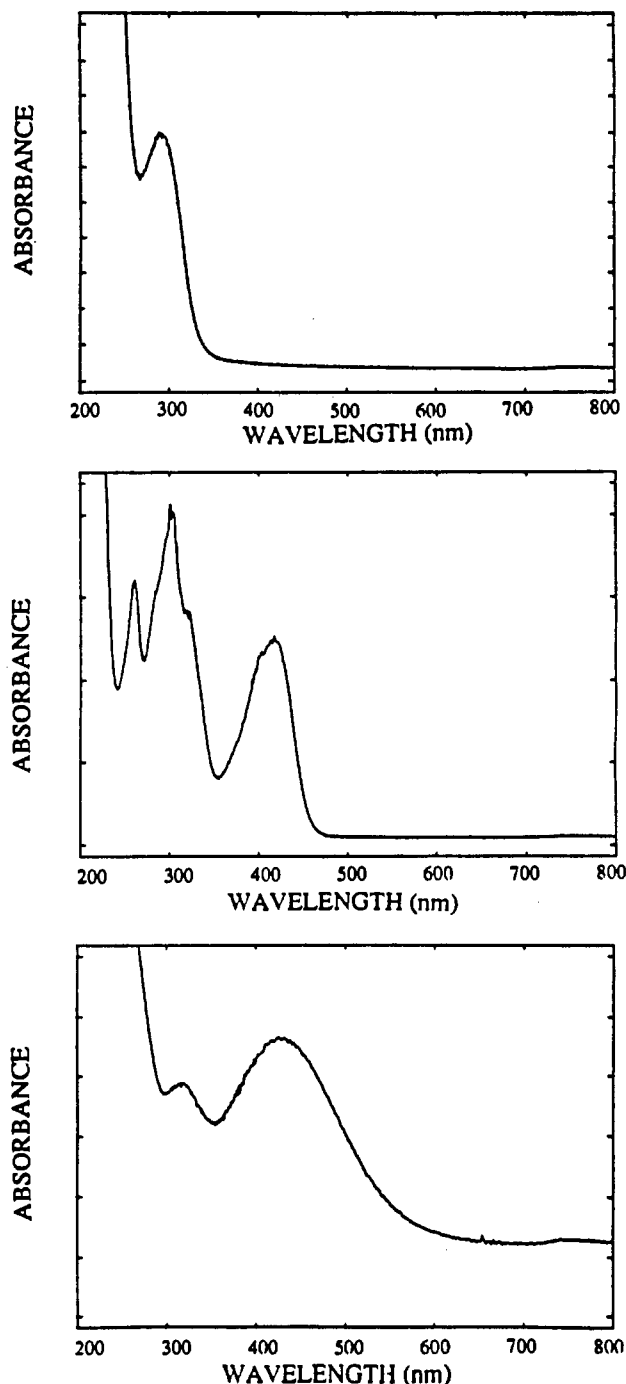


Figure 1. UV-vis absorption spectrum of (a, top) $Pt(NH_3)_4(NO_3)_2$, (b, middle) $K_3Fe(CN)_6$, and (c, bottom) $C_{12}H_{12}Fe_2N_{16}Pt(N_4H_{12}Pt)_2 \cdot 9H_2O$ in distilled water.

formation, changes also occur in the 1400- cm^{-1} NH_3 bending region with a single peak at 1380 cm^{-1} for tetraammineplatinum(II) nitrate splitting into a multiplet of peaks having significantly lower intensity.

Two broad peaks occur in the UV-vis spectrum of this compound at 318 and 424 nm with molar absorptivities of 2090 and 2365 $M^{-1} cm^{-1}$, respectively (see Figure 1). The higher energy peak is most likely a simple addition of the platinum and iron complex transitions. The transition at 424 nm can be distinguished from the ferricyanide $d\pi-Fe \rightarrow \pi^*-CN$ MLCT band at 416 nm due to the red shift in the tail of the band associated with the new complex. This can be seen in a comparison of parts b (ferricyanide spectrum) and c (product spectrum) of Figure 1. It is this tail

(7) Sheldrick, G. M. SHELXTL. An Integrated System for Solving, Refining and Displaying Crystal Structures from Diffraction Data. University of Göttingen, Federal Republic of Germany, 1980.

(8) Cromer, D. T.; Waber, J. T. *International Tables for X-Ray Crystallography*; Kynoch Press: Birmingham, England, 1974; Vol. IV.

(9) Dows, D. A.; Haim, A.; Wilmarth, W. K. *J. Inorg. Nucl. Chem.* **1961**, *21*, 33.

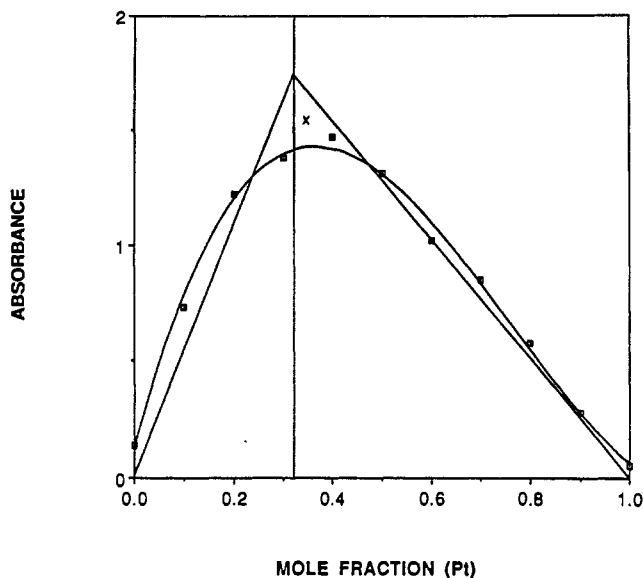
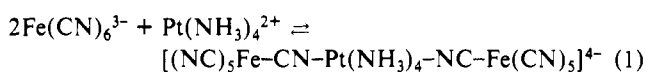


Figure 2. Job plot depicting the 2:1 Fe/Pt ratio for $C_{12}H_{12}Fe_2N_{16}Pt(N_4H_{12}Pt)_2 \cdot 9H_2O$ in solution with absorbance monitored at 472 nm. The stability constant can be estimated from the value of x .

that gives the diagnostic red color to the solution species. However, because of the spectral overlap of the ferricyanide reagent and the product absorption band, it is impossible to ascertain purely from the UV-visible spectrum whether or not the $d\pi$ -Fe $\rightarrow \pi^*$ -CN MLCT transition exists in the product complex. That is, the new transition centered at 424 nm could account for all of the absorptivity in the 400–500-nm region of the spectrum. It is clear, however, from a comparison of Figure 1b,c that the spectral absorbance at wavelengths greater than 465 nm is solely due to the product complex. Thus, this spectral region was employed to investigate the structural and thermodynamic properties of the product species. Using the Job¹⁰ method (as shown in Figure 2) to analyze the absorptivity at 472 nm as a function of the ratio of $Fe(CN)_6^{3-}$ to $Pt(NH_3)_4^{2+}$ in solution indicates a stoichiometry for the product of 2:1 (Fe:Pt). An equilibrium stability constant of 10^6 is also approximated from these data by using several Job plots at differing total concentrations. On the basis of the IR and UV-visible spectroscopic data, the overall reaction is considered to be



$$\frac{[(NC)_5Fe-CN-Pt(NH_3)_4-NC-Fe(CN)_5]^{4-}}{[Fe(CN)_6^{3-}]^2[Pt(NH_3)_4^{2+}]} = 10^6 \quad (2)$$

Redox Chemistry and Oxidation States. Cyclic voltammograms taken in 1 M $NaNO_3$ by using Pt working and counter electrodes show a single redox event with $E_{1/2} = +0.60$ V versus SCE (see Figure 3). It should be noted that this redox potential is shifted positive about 380 mV from that of the ferro/ferricyanide couple. In the scan rate range from 20 to 300 mV/s, the cyclic voltammogram is invariant with respect to the current function ($i_p/\omega^{1/2}$) and peak to peak separation. Since only one redox wave was observed, the possibility of a simultaneous two-electron oxidation, one electron coming from each iron center, was speculated. To test this hypothesis, an equimolar amount of $Ru(NH_3)_6^{3+}$ was added to the electrochemical cell as a one-electron standard at pH = 7. The peak anodic current for the $[Ru(NH_3)_6]^{2+/3+}$ cyclic voltammogram was half of that observed for the trinuclear complex. Since the complex of interest has a diffusion coefficient¹¹ similar to that of $Ru(NH_3)_6^{3+}$ (see below), the two-electron nature of the redox reaction was confirmed. Such a process would be expected to yield a 30-mV peak to peak separation; however, 120

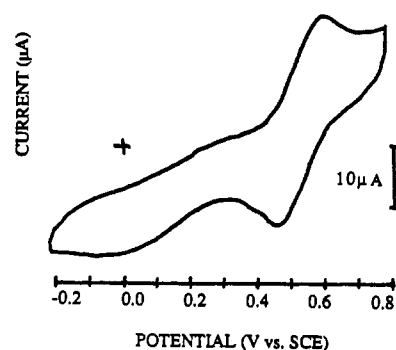


Figure 3. Cyclic voltammogram of $C_{12}H_{12}Fe_2N_{16}Pt(N_4H_{12}Pt)_2 \cdot 9H_2O$ in 1 M KNO_3 at 100 mV/s scan rate taken by using a Pt working and counter electrode with an SCE reference electrode.

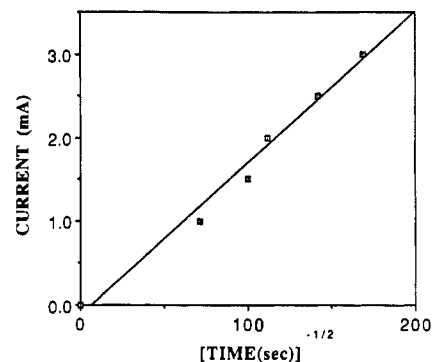


Figure 4. Chronoamperometry study of $C_{12}H_{12}Fe_2N_{16}Pt(N_4H_{12}Pt)_2 \cdot 9H_2O$ in 0.5 M $NaNO_3$ depicting current as a function of $(\text{time})^{-1/2}$.

mV is observed for the complex compared to 70 mV for the $Ru^{2+/3+}$ couple. This suggests that the former redox process is quasi-reversible under these pH conditions (the ferro/ferricyanide couple is also known to be quasi-reversible in the pH = 5–7 range).

The cyclic voltammetric data are indicative of an Fe^{II} - Pt^{IV} - Fe^{II} initial oxidation state producing an Fe^{III} - Pt^{IV} - Fe^{III} product upon electrochemical oxidation. Further, the observation of a single cyclic voltammetric wave for the oxidation of both iron centers provides strong evidence that the two iron sites are not in charge-transfer communication. Electron spin resonance and magnetic susceptibility measurements revealed no unpaired electrons, adding further evidence for the oxidation state assignment given above. As mentioned previously, the IR terminal cyanide stretching frequency also resembles that of ferrocyanide as opposed to ferricyanide.

A chronoamperometric study was performed in the potential range from 0.3 to 0.8 V vs SCE. In this potential range, the system was found to exhibit Cottrellian behavior, as displayed in Figure 4, consistent with the cyclic voltammetric conclusion of reversibility. From these data, a diffusion coefficient of $3 \times 10^{-6} \text{ cm}^2 \text{ s}^{-1}$ was extracted.

It is interesting to note that the complex forms via a redox expansion of the coordination sphere of platinum from Pt^{II} to Pt^{IV} . This is likely the reason that the reactants form a trinuclear compound as opposed to a longer chain oligomer or polymer. That is, the product stoichiometry is controlled by the necessity of a two-electron transfer, and therefore, exactly two one-electron reagents are incorporated into the product species. It is speculated that the reaction of ferrocyanide with a labile Pt^{IV} compound might directly form a polymeric species similar to Prussian blue, linked via cyanide bridges. The characterization of the precipitate from such a reaction is currently under investigation in our laboratory.

Crystal Structure. A summary of crystallographic data appears in Table I. The ORTEP plot is shown in Figure 5, and the unit cell is depicted in Figure S1 in the supplementary material. The final R factor for the structure was 5.0% and the weighted value, R_w , was 5.3% (equations used are listed in Table S1 in the supplementary material). The identical Fe–Pt bond distances in the crystal structure of the trinuclear anion confirm the conclusion

(10) Vosburgh, W. C.; Cooper, G. R. *J. Am. Chem. Soc.* **1941**, *63*, 437.
 (11) Nicholson, R. S.; Shain, I. *Anal. Chem.* **1964**, *36*, 706.

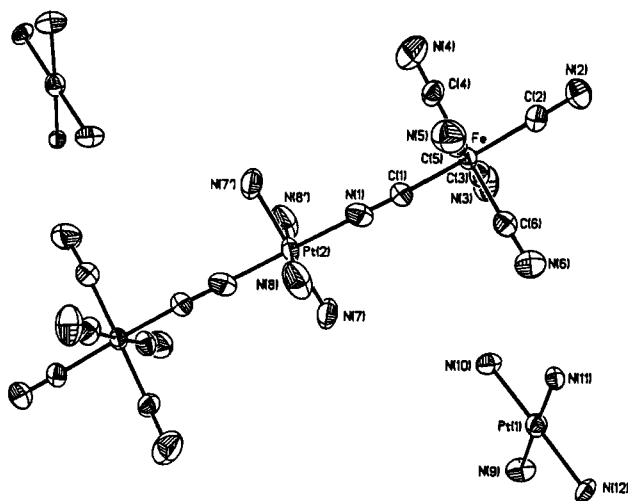


Figure 5. ORTEP drawing for the single-crystal X-ray study of $C_{12}H_{12}Fe_2N_{16}Pt(N_4H_{12}Pt)_2 \cdot 9H_2O$ using a Nicolet R3m diffractometer.

Table I. Crystal Structure Determination Summary

empirical formula	$C_{12}H_{12}Fe_2N_{16}Pt(N_4H_{12}Pt)_2 \cdot 9H_2O$
unit cell dimens	$a = 15.313 (2) \text{ \AA}$ $b = 8.5353 (14) \text{ \AA}$ $c = 16.206 (5) \text{ \AA}$ $\alpha = 90.0^\circ$ $\beta = 100.52 (2)^\circ$ $\gamma = 90.0^\circ$
V	$2082.5 (7) \text{ \AA}^3$
Z	2
fw	1375.8
space group	$P2_1/c$ (No. 14)
temp	25°C
radiation	Mo $K\alpha$ ($\lambda = 0.71069 \text{ \AA}$)
density (calcd)	2.19 g/cm^3
abs coeff	113.3 cm^{-1}
transm coeff	0.165–0.690
R, R_w	5.0%, 5.3%

that the two Fe centers bear the same oxidation number. The molecular unit consists of a net 4[−] anion constructed from two ferrocyanides spanned by tetraammineplatinum(IV) via cyanide bridges; two $Pt(NH_3)_4^{2+}$ counterions, along with nine waters of hydration, complete the molecular structure. Selected bond distances are listed in Table II; Table III summarizes the atomic coordinates. The average nearest-neighbor N–Pt–N and C–Fe–C bond angles are essentially 90° , with the Pt–N–C and Fe–C–N bond angles approximately 180° . As can be seen from the ORTEP plot, the two counterions sit close to the terminal Fe atoms, not the Pt^{IV} center of inversion. It is likely that two of the ammine groups on each counterion are hydrogen-bonded to the nitrogen on a terminal cyanide group of the iron. The N(6)–N(10) and N(6)–N(11) distances are 2.976 (19) and 2.948 (13) Å, respectively, within hydrogen-bonding distance. We speculate that this hydrogen-bonding interaction allows the formation of high-quality crystals with relative ease. Consistent with this conclusion we find that Ni^{2+} , Zn^{2+} , and $[Ru(bpy)_3]^{2+}$ can be used in place of $[Pt(NH_3)_4]^{2+}$ in the counterion positions to make powdered solids; however, crystallization is poor in these systems. An elaborate network of hydrogen bonding involving the waters of hydration and the platinum ammine groups is also established by the X-ray structure but is not shown in the ORTEP plot for simplicity's sake. Interestingly, most of the waters reside about the central platinum(IV) in the trinuclear structure. Upon dehydration in vacuo or by gentle heating, as well as by addition of hydrophilic solvents such as acetone to the red-orange precipitate, the solid turns black. This color change is reversible upon exposure to humid air or redissolution in distilled water. The recovered solid has physical properties and electronic and infrared spectra identical with those of the original compound. Therefore, we conjecture that removing the waters of hydration around the central Pt^{IV} atom allows the Pt^{II} counterions to move close enough to the trinuclear anion to

Table II. Selected Bond Distances (Å) for $C_{12}H_{12}Fe_2N_{16}Pt(N_4H_{12}Pt)_2 \cdot 9H_2O$

Pt(1)–N(9)	2.062 (10)	Pt(1)–N(10)	2.065 (10)
Pt(1)–N(11)	2.045 (9)	Pt(1)–N(12)	2.054 (10)
Pt(2)–N(1)	1.971 (11)	Pt(2)–N(7)	2.076 (11)
Pt(2)–N(8)	2.072 (13)	Fe–C(2)	1.948 (11)
Fe–C(1)	1.883 (12)	Fe–C(3)	1.931 (13)
Fe–C(4)	1.891 (11)	Fe–C(5)	1.914 (13)
Fe–C(6)	1.937 (12)	C(1)–N(1)	1.14 (2)
C(2)–N(2)	1.12 (2)	C(3)–N(3)	1.15 (2)
C(4)–N(4)	1.17 (2)	C(5)–N(5)	1.14 (2)
C(6)–N(6)	1.14 (2)		
Pt(1)–Pt(2)	7.479 (1)	N(6)–N(10)	2.976 (19)
Fe–Pt(2)	4.993 (1)	N(7)–N(10)	4.293 (11)
Fe–Pt(1)	6.769 (2)	N(6)–N(11)	2.948 (13)

Table III. Atomic Coordinates ($\times 10^4$) and Isotropic Thermal Parameters ($\text{\AA}^2 \times 10^3$) for $C_{12}H_{12}Fe_2N_{16}Pt(N_4H_{12}Pt)_2 \cdot 9H_2O$

	x	y	z	U^a
Pt(1)	991 (1)	7488 (1)	−3801 (1)	34 (1)
Pt(2)	5000	5000	0	38 (1)
Fe	2315 (1)	1573 (2)	−357 (1)	31 (1)
C(1)	3317 (8)	2892 (13)	−216 (7)	36 (4)
N(1)	3921 (7)	3695 (12)	−134 (7)	49 (4)
C(2)	1315 (7)	126 (13)	−520 (7)	34 (3)
N(2)	761 (7)	−754 (13)	−642 (6)	46 (4)
C(3)	1743 (8)	2899 (13)	351 (8)	40 (4)
N(3)	1409 (8)	3724 (14)	762 (7)	60 (4)
C(4)	2867 (8)	413 (13)	590 (7)	38 (4)
N(4)	3179 (9)	−320 (15)	1184 (9)	72 (5)
C(5)	2859 (8)	311 (13)	−1098 (8)	41 (4)
N(5)	3174 (9)	−412 (14)	−1553 (8)	63 (5)
C(6)	1722 (9)	2778 (12)	−1309 (8)	40 (4)
N(6)	1349 (9)	3504 (15)	−1854 (8)	66 (5)
N(7)	4220 (8)	6958 (13)	−363 (9)	61 (5)
N(8)	5090 (9)	4499 (16)	−1233 (8)	67 (5)
N(9)	852 (10)	9781 (11)	−2727 (7)	59 (5)
N(10)	1605 (9)	6960 (12)	−1870 (6)	53 (4)
N(11)	1107 (7)	5222 (10)	−3458 (7)	45 (4)
N(12)	381 (7)	8061 (12)	−4280 (7)	45 (3)
O(1)	2528 (10)	6591 (15)	66 (11)	117 (8)
O(2)	4978 (10)	−1010 (18)	1106 (14)	141 (9)
O(3)	3349 (14)	−235 (37)	2907 (12)	254 (18)
O(4)	4949 (24)	2882 (31)	6849 (18)	230 (19)
O(5)	3415 (20)	4103 (71)	1868 (17)	238 (27)

^a Equivalent isotropic U defined as one-third of the trace of the orthogonalized U_{ij} tensor.

establish a series of $Pt^{II} \rightarrow Pt^{IV}$ IT transitions in the visible spectrum. Since we find the dehydrated material to be insoluble in all solvents (except water), we cannot confirm this finding spectroscopically.

Photophysics and Photochemistry. The unique absorption in the electronic spectrum (centered at 424 nm) and the color change upon reaction is assigned as an intervalent (IT) charge transfer from Fe^{II} to Pt^{IV} . No possibility of a LMCT band based purely on the cyanoiron moiety exists (such as that observed in Figure 1b), since ferrocyanide has no absorptivity in this spectral region. Furthermore, as discussed in the introduction, the possibility of a MLCT transition from the platinum center to the π^* of the cyanide ligands would occur at significantly higher energies.³

Irradiation into the IT charge-transfer band of the complex in solution using 488-nm light from an Ar ion laser yields a yellow solution with an electronic spectrum exactly matching that of ferrocyanide. The quantum yield for the formation of ferrocyanide was determined to be 0.02 with 488-nm irradiation. This value is relatively wavelength independent over the range 460–560 nm (data were collected every 20 nm).¹² The photolysis process is reversed in the dark as indicated by eq 1. At high complex

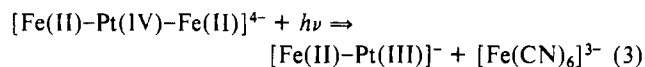
(12) The quantum yield determination was made by using solutions sufficiently dilute that the thermal back-reaction to re-form the complex occurred to a negligible extent over the time period necessary to obtain an UV–visible spectrum of the photolyzed solution.

concentrations, the photoreaction does not appear to occur, presumably because the back-reaction proceeds faster than the photolysis. Likewise, at sufficiently low concentrations the back-reaction of the photolyzed complex is not observed. Titration of the resultant yellow solution (at concentrations where the back-reaction is negligible) with ferrous sulfate yielded Prussian blue, which was then filtered out of the solution. The remaining filtrate showed a UV-vis absorption at the same wavelength as that of $\text{Pt}(\text{NH}_3)_4(\text{NO}_3)_2$. These results demonstrate that the starting products are regenerated upon photolysis by irradiation into the IT band. Others have reported charge-transfer photo-reactions for binuclear cyanide-bridged species.⁴ Vogler, for example, demonstrated that the photolysis of $[(\text{NC})_5\text{Co}^{\text{III}}-\text{NC}-\text{Os}^{\text{II}}(\text{CN})_5]^{6-}$ leads via photoinduced electron transfer to the reactants from which it was formed by a thermal reaction, namely $[\text{Co}^{\text{II}}(\text{CN})_5]^{3-}$ and $[\text{Os}^{\text{III}}(\text{CN})_6]^{3-}$.^{4c} However, to the best of our knowledge, the observation of a photoinduced two-electron charge-transfer based on a MMCT transition, as observed in the current case, has not previously been observed.

Conclusions

Since all of the photochemical experiments described were carried out at low light intensity (i.e. $<75 \text{ mW/cm}^2$) the possibility of a multiphoton event leading to a simultaneous two-electron charge transfer can be ruled out. Further, the electrochemical

data indicating that the two iron centers are noninteracting rule out the presence of a ground-state molecular orbital, delocalized over the entire trinuclear complex, from which a photoinduced two-electron charge transfer might occur. Therefore, the most likely mechanistic pathway leading to the observed two-electron charge-transfer chemistry involves an initial one-electron excitation from one of the two iron centers to generate an excited-state $\text{Pt}(\text{III})$ species followed by a thermal charge transfer to form the observed products as follows:



Acknowledgment. This work was supported by the National Science Foundation under Grant No. CHE-8700868. B.W.P. is grateful for a General Electric Fellowship covering part of the duration of this research.

Supplementary Material Available: Tables SI-SV, listing additional crystal structure determination parameters, all nonequivalent bond distances and bond angles, atomic coordinates and isotropic thermal parameters, and anisotropic thermal parameters, and Figure S1, depicting the unit cell under the conditions listed in the Experimental Section (7 pages); Table SVI, listing observed and calculated structure factors (17 pages). Ordering information is given on any current masthead page.

Contribution from the Department of Inorganic Chemistry, Royal Institute of Technology, S-10044 Stockholm, Sweden

Inner- and Outer-Sphere Complex Formation in Aqueous Erbium Halide and Perchlorate Solutions. An X-ray Diffraction Study Using Isostructural Substitution

Georg Johansson* and Haruhiko Yokoyama†

Received August 18, 1989

Intensity difference functions obtained from large angle X-ray diffraction measurements on isostructural erbium and yttrium halide and perchlorate solutions have been used to derive the coordination around the erbium ion in solutions of different concentrations and anion-metal ratios. Two well-defined coordination spheres can be distinguished in the radial distribution functions. In the first sphere the erbium ion coordinates $8.0 \pm 0.3 \text{ H}_2\text{O}$ molecules at a distance of $2.35 \pm 0.01 \text{ \AA}$. Halide ions and possibly perchlorate ions penetrate into this sphere only when present in very large concentrations. In the inner-sphere complexes then formed, the Er-Cl and the Er-Br bonding distances are found to be 2.7 ± 0.1 and $2.87 \pm 0.02 \text{ \AA}$, respectively. The halide ions are concentrated to the second coordination sphere, in which the ratio between the numbers of halide ions and water molecules is larger than the stoichiometric ratio. In these solvent-separated ion pairs (outer-sphere complexes), the Er-Cl and Er-Br distances are found to be 5.0 \AA .

Introduction

The structures of the solvated lanthanide ions and their complexes in solution have been the subject of a large number of investigations. Most methods, however, are capable of giving only indirect evidence on the nature of the bonding between the metal ions and their ligands. Direct structural information can be obtained with the use of diffraction methods, which give radial distribution functions (RDF), from which the structures of the solvated ions and their complexes can be derived. The information on the structures, contained in the RDFs, is usually, however, obscured by other structural features of the solution, which can prevent an unambiguous determination of the structure around the metal ion. In an aqueous solution, for example, water-water distances often appear in the same region as metal-water and metal-ligand distances, and the contributions of the different types of interactions to the scattering data cannot easily be resolved.

By the use of scattering measurements from two isostructural solutions, containing metal ions with different scattering powers, the non-metal interactions, which are the same in the two solutions,

can be eliminated and the part of the RDF involving the metal ions can be separated.^{1,2} The coordination can then be studied independently of the remaining structure. For the lanthanides, yttrium can be used for this purpose. The three-valent lanthanide ions and the yttrium ion all have the same outer electron configuration and differ only in the number of 4f electrons. They interact mainly electrostatically with their surroundings, and the f electrons contribute little to the bonding. The chemical differences result primarily from the slight decrease in ionic radius with increasing atomic number. In its chemical characteristics, yttrium usually appears among the heavy lanthanoids close to Ho^{3+} and Er^{3+} . Their thermodynamic characteristics do not usually differ significantly, their ionic radii are nearly the same, and their crystal structures are isomorphous and usually show no significant differences between observed bond lengths. X-ray diffraction measurements on solutions of these ions support the assumption that they are isostructural.^{3,4} In the present work, the Y-Er pair

* Present address: Department of Chemistry, Yokohama City University, Seto, Kanazawa-ku, Yokohama 236, Japan.

- (1) Bol, W.; Gerrits, G. J. H.; vanEck, C. L. v. P. *J. Appl. Crystallogr.* **1970**, *3*, 486.
- (2) Soper, A. K.; Neilson, G. W.; Enderby, J. E.; Howe, R. A. *J. Phys. C* **1977**, *10*, 1793.
- (3) Johansson, G.; Wakita, H. *Inorg. Chem.* **1985**, *24*, 3047.